PERGAMON

International Journal of Heat and Mass Transfer 44 (2001) 3997–4007

International Journal of HEAT and MASS TRANSFER

www.elsevier.com/locate/ijhmt

Optimum jet-to-jet spacing of heat transfer for staggered arrays of impinging air jets

Jung-Yang San *, Mao-De Lai

Department of Mechanical Engineering, National Chung Hsing University, 250 Kuo-Kuang Road, Taichung 40227, Taiwan, ROC

Received 12 September 2000; received in revised form 10 January 2001

Abstract

The effect of jet-to-jet spacing on the local Nusselt number for confined circular air jets vertically impinging on a flat plate is investigated. Five jets in equilaterally staggered arrays are considered. The surface heat flux on the plate is 1500 W m^{-2}. The jet diameter is 3 mm. Three different jet Reynolds numbers ($Re = 10{,}000$, 20,000 and 30,000) are individually considered. The influence of jet-to-jet spacing, Re and jet height on the stagnation Nusselt number of the center jet is experimentally investigated. An optimum ratio of jet-to-jet spacing to jet diameter, $(s/d)_{opt}$, is obtained. The existence of the $(s/d)_{opt}$ is attributed to jet interference before impingement and/or formation of jet fountain between two adjacent jets. The stagnation Nusselt number is correlated as a function of Re, s/d and H/d. © 2001 Elsevier Science Ltd. All rights reserved.

Keywords: Jet; Impingement; Nusselt number; Stagnation point

1. Introduction

Jet impingement can be found in many engineering applications. In steel or glass industry, impinging jets are applied to temper products after rolling. In gas turbine engines, impinging jets are used in cooling of turbine vanes. Recently, jet impingement cooling has been applied to electronic devices in order to meet the demand of compactness and high power consumption. Besides the above applications in cooling, impinging jets are also adopted in paper industry to enhance drying processes.

The flow field of a confined axisymmetric impinging jet was studied experimentally by Garimella et al. [1] and Fitzgerald et al. [2]. In their work, a toroidal recirculation flow was mapped and the stagnation Nusselt number was expressed as a function of Reynolds number, Prandtl number, jet hole aspect ratio and jet height. Many other researches related to impingement heat transfer of a single jet are elaborated by Garimella et al. [1], Fitzgerald et al. [2] and San et al. [3]. Similarly, a large amount of work related to impingement heat transfer of multiple jets is also available. Gardon et al. [4] investigated the heat transfer characteristics of two-dimensional air jets impinging perpendicular to an isothermal flat plate. The average Nusselt number of a square in-line array of confined circular air jets impinging perpendicular to a flat plate was obtained by Kercher et al. [5]. The heat transfer characteristics for several in-line and staggered arrays of circular air jets impinging on an isothermal plate were investigated by Metzger et al. [6] and Florschuetz et al. [7–12]. Some of their results will be compared with the data obtained in this work.

Saripalli [13] conducted a flow visualization of multiple jet impingement. A fountain between two adjacent jets was observed. The interaction between the fountain and the two jets was found to increase with decreasing the jet spacing. The local Nusselt number for staggered arrays of circular air jets impinging on a constant heat flux surface was obtained by Behbahani et al. [14]. A relative maximum of Nusselt number, between two adjacent jets in the streamwise direction, was clearly observed. The occurrence of this maximum is attributed to an increase of the turbulence intensity resulting from the interaction of the two jets. Glodstein

* Corresponding author. Tel.: +886-4-2284-0432; fax: +886-4-2285-1941.

E-mail address: jysan@drangon.nchu.edu.tw (J.-Y. San).

PII: S0017-9310(01)00043-6

Nomenclature

a_{ijk}	coefficients
c_{ij}	functions of Re
d	jet hole diameter (mm)
h	convective heat transfer coefficient (W m^{-2} K^{-1})
H	distance from jet exit to impingement plate (mm)
k	thermal conductivity of air (W m^{-1} K^{-1})
Nu	local Nusselt number, hd/k
q	surface heat flux (W m^{-2})
Q	volumetric flowrate (m^3 s^{-1})
Re	Reynolds number, $4Q/\pi\nu$d
s	jet-to-jet spacing (mm)
T_{aw}	adiabatic wall temperature (°C)
T_j	jet total temperature (°C)
T_w	heated wall temperature (°C)
W	width of heated area (mm)
x	streamwise coordinate (mm)
y	coordinate perpendicular to streamwise direction (mm)

Greek symbols

α	power of Reynolds number
α_1, α_2	functions of H/d
β_i, γ_i	coefficients
ν	kinematic viscosity (m^2 s^{-1})

Subscripts

opt	optimum value
sg	stagnation point of center jet

et al. [15] used a liquid crystal system to visualize the isotherms on a heated plate which is exerted with a multijet impingement cooling. This technique can clearly characterize the heat transfer of a jet array. Slayzak et al. [16] investigated the effect of jet interaction on the local heat transfer for two-dimensional impinging jets. A maximum convective heat transfer coefficient between two stagnation lines was found. The existence of this maximum, as explained in the above, is due to the jet fountain. Huber et al. [17,18] investigated the effect of jet-to-jet spacing on the convective heat transfer to in-line arrays of circular air jets. The result reveals that the local Nusselt number decreases with the jet-to-jet spacing. For a fixed jet-to-jet spacing, the adjacent jet interference before impingement reduces as the jet height decreases.

Although there were many research works dealing with impingement heat transfer of jet arrays, as a whole, there are still many blind spots which need to be clarified. In this work, the distribution of local Nusselt number for five confined circular air jets in staggered arrays vertically impinging on a flat plate is experimentally determined. The effect of jet-to-jet spacing on the stagnation Nusselt number of the center jet is investigated for various Reynolds numbers and jet heights. It is intended to obtain a design strategy of jet-to-jet spacing for staggered arrays of confined impinging air jets.

2. Local Nusselt number

In this work, five impinging jets in staggered arrays are considered (Figs. 1 and 2). The local convective heat transfer coefficient, h, between the jet flow and impingement plate is defined as follows:

$$h = \frac{q}{(T_w - T_{aw})} \tag{1}$$

In Eq. (1), both the T_w and T_{aw} are locally measured. In many cases, $(T_j - T_{aw})$ is small. Thus this temperature difference can be neglected and the adiabatic wall temperature, T_{aw}, in Eq. (1) can be replaced by the jet total temperature, T_j.

In the experiment, the jet hole diameter, d, is 3 mm. The ratio of heated width to jet diameter, W/d, is 29.17. The orifice aspect ratio is 1.0 and the surface heat flux, q, is 1500 Wm^{-2}. The local Nusselt number in the flow direction ($y = 0$) can be expressed as a function of several variables as follows:

$$Nu = Nu(H/d, x/d, Re, s/d) = \frac{qd}{k(T_w - T_{aw})} \tag{2}$$

The parameters, H/d, x/d, Re and s/d, are treated as the variables in the measurement. In Eq. (2), the thermal conductivity of air, k, is 0.026 W m^{-1} K^{-1}. In this work, for the sake of brevity, the local Nusselt number at the stagnation point of the center jet ($x = y = 0$), Nu_{sg}, is used to represent the overall heat transfer of the corresponding jet array.

3. Apparatus and experimental procedure

Fig. 3 shows the experimental set-up for the measurement. The high-pressure air is supplied by a large reciprocating air compressor. The air pressure in the compressor tank is in the range of 5–6 kg cm^{-2}. A pressure regulator is installed at the exit of the tank to control the exit air pressure. The high-pressure supplied air needs to be purified before it is used for impingement cooling. This is done by installing a vapor compression type dehumidifier for dehydration and by installing several adsorption columns filled with activated carbon particles for oil removal in the air supply line. The dehumidified air is stored in a large surge tank in which the

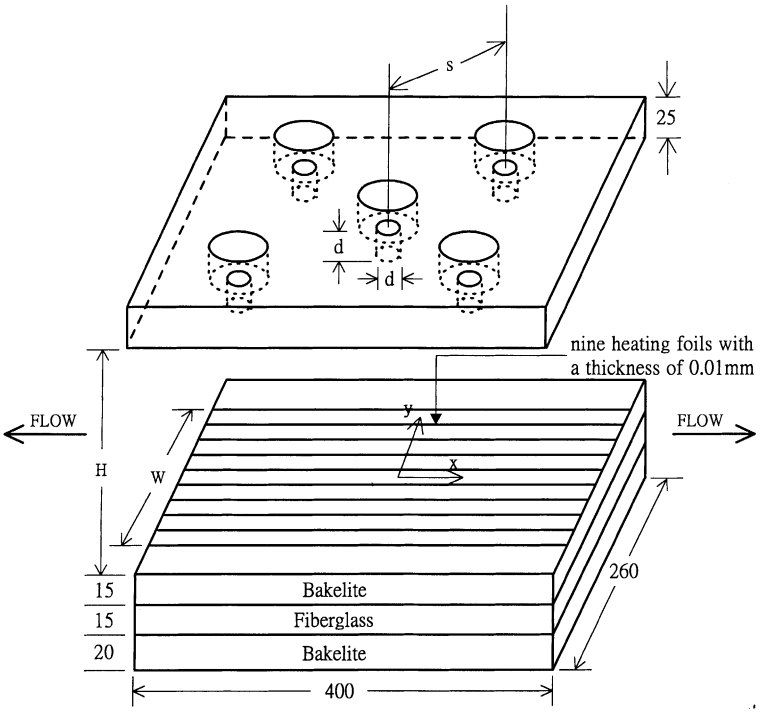

Fig. 1. Impingement plate and jet plate.

pressure is maintained at 3 kg cm^{-2}. The function of the surge tank is to diminish the pressure fluctuation due to the on–off cycling of the air compressor. A pressure regulator is installed at the exit of the tank to control the exit air pressure. In order to reduce the temperature variation of the supplied air, a temperature-controlled water bath embedded with a heat exchanger coil is installed. In doing so, both the temperature variation of the water and the temperature variation of the high-pressure air are controlled within 0.2°C.

Both liquid crystal technique and infrared technique are widely applied to measure temperature distributions on solid surfaces. For two-dimensional measurements, these two techniques provide researchers not only with a continuous temperature map, but also with a short measuring time. Nevertheless, the obtained data from these two techniques quantitatively are not as accurate as those obtained from traditional thermocouple technique. Thus in this work, instead of using liquid crystal technique and infrared technique, a thin T-type thermocouple is adopted to measure the local temperature on the impingement plate.

The jet plate and the impingement plate are shown in Fig. 1. The width of the two plates is 260 mm and the length is 400 mm. The air in the channel is restricted to flow only in two opposite directions as shown in Fig. 1. Nine 0.01 mm thickness stainless steel heating foils are attached to the impingement plate by using a non-conductive adhesive. The width of the heating foil is 12.5 mm and the length is 400 mm. The discontinuities between two neighboring heating foils are filled with a silicon material to produce a smooth impingement surface. The joint between the heating foil and the electricity wire is carefully soldered to access a negligible voltage drop. The resistance of every heating foil is carefully examined to ensure the heating is uniform on the surface.

Seventy-six T-type thermocouples are embedded beneath the middle heating foil. The spacing between any two neighboring thermocouples is 3 mm. The diameter of the thermocouples is 0.1 mm and the bead is less than 0.25 mm. Besides the adhesive layer, a thermally well-conductive paste is applied between the heating foil and the thermocouple beads. The paste is also dielectric. This insures that the signals of the thermocouples are not disturbed by the electricity on the heating foil. A d.c. electric current is conducted to heat the foils with a uniform heat generation rate. The supplied power to the heating foils is measured by using a digital power meter. The heating foils are stuck on a bakelite plate which has a thickness of 15 mm. Below the bakelite plate, there is a 15 mm thickness fiberglass insulation. At the bottom of the impingement plate structure, there is another bakelite plate with a thickness of 20 mm to support the insulation. The jet plate is made of acrylic. To reduce the heat loss from the jet plate, it is covered with a 20 mm thickness PS foam.

In this experiment, the jet plate can be moved in the x and y directions individually by adjusting two screws.

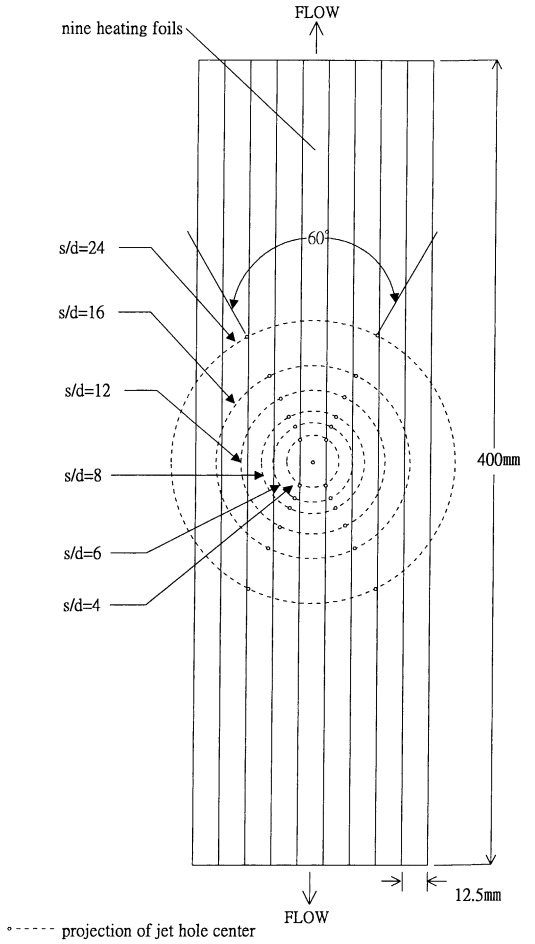

Fig. 2. Projection of jet hole centers on impingement plate.

The jet plate is positioned by using two linear photoelectronic scales, which provide a smallest readout of 0.001 mm. In the present work, only one thermocouple is used throughout the entire measurement. In doing so, the inaccuracy of the temperature measurement can be minimized. The measurement is conducted in a room with air conditioning. In such an arrangement, the room temperature can be controlled within a deviation of 1.5°C from the jet total temperature. During the operation, a long time period is needed for the system to reach a thermally steady-state condition. In this work, a waiting period of 3 h is set at the beginning of every adiabatic or heated wall measurement. After that, for every point measurement, there is a waiting period of 10–15 min. The temperature of the measured point is recorded by a HP-3497 data acquisition system. The obtained data are analyzed by using a personal computer.

A turbine flowmeter (EG & G) is installed in the air supply line. The turbine flowmeter is used to calibrate five pressure gauges for every measured Reynolds number. The calibrations are performed individually for every pressure gauge. Once the calibrations between the pressure and Reynolds number for the five air lines are done, the valves in front and after the turbine flowmeter will be closed. The flow is then bypassed in a tube directly to the corresponding pressure gauge and jet hole plate. In doing so, the flowrates of the air jets can be accurately controlled by observing the scales on the pressure gauges.

4. Error analysis

In this work, a high accuracy of the measurement is demanded. The uncertainty of the experiment mainly results from the measurement of jet mass flowrate and that of convective heat transfer coefficient. The former is due to the inaccuracy of the turbine flowmeter. According to the manufacturer's supplied data, this inaccuracy is assured to be within 1%. The inaccuracy of the latter is attributed to the heat flux error and temperature error in the measurement. The surface heat flux on the heating foils is mainly affected by radiation loss, non-uniformity of heating foil, lateral solid heat conduction and heat loss through insulation. The temperature error results from two reasons. One is the thermal resistance of epoxy resin between the center heating foil and thermocouples. The other is related to the quality of the thermocouples. By performing a detailed analysis, the maximum possible errors due to the above factors are individually obtained as follows:

A. Heat flux error:
   (i) radiation loss: 2.5%
   (ii) non-uniformity of the heating foil: 4.3%
   (iii) lateral solid heat conduction: 0.7%
   (iv) heat loss through insulation: 0.6%

B. Temperature error:
   (i) thermal resistance of epoxy resin: 0.01 K
   (ii) inaccuracy due to thermocouple: 35 ± 0.2°C

In evaluation of the convective heat transfer coefficient, only the difference of the adiabatic wall temperature and heated wall temperature is needed. In this work, the same thermocouple is used to measure these two temperatures, thus the inaccuracy of the temperature measurement is reduced. Neglecting the error in the temperature measurement, the uncertainty of the Nusselt number in this experiment is less than 5.1%.

5. Results

From the results of Saripalli's flow visualization [13], the heat transfer of an impinging jet array is believed to be strongly affected by jet interference before impingement and/or jet fountain. The jet interference before impingement, as shown in Fig. 4, happens in the case

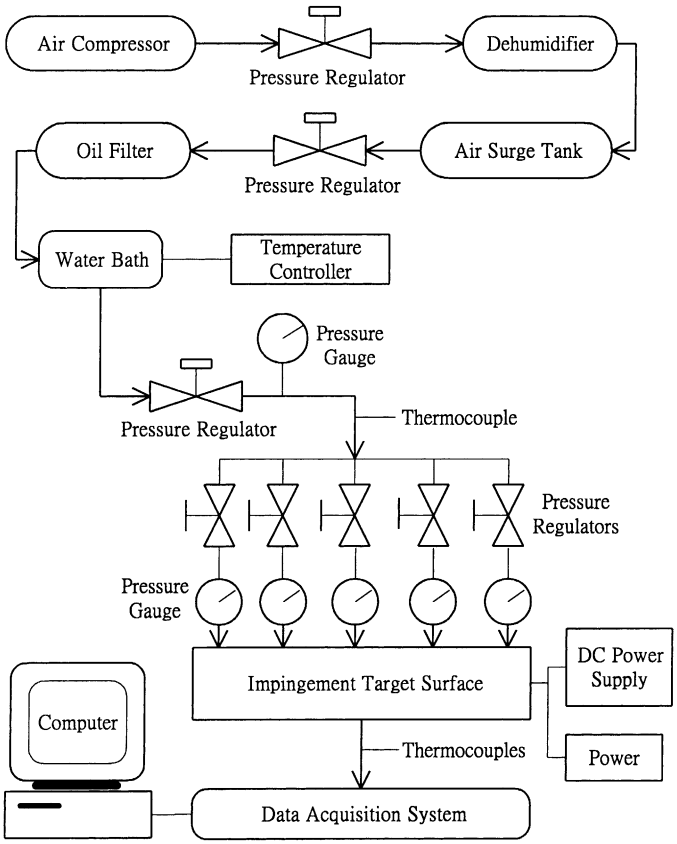

Fig. 3. Experimental apparatus.

with a small jet spacing. For a small jet spacing, due to shear layer expansion, an interference between two adjacent jets will occur before impingement. This interference would weaken the jet strength and eventually degrade the heat transfer of the jet array. The jet fountain, as shown in Fig. 5, is mainly attributed to the face-to-face encounter of the two adjacent wall jets. If the strength of this interaction is strong, a fountain will form between the two jets. Due to entrainment effect, both the flow on the right side and the flow on the left side of the fountain will recirculate and thus the heated air will reenter the core of the jets. This will also affect the heat transfer of the jet array. In this work, the effects of jet interference before impingement and jet fountain on the heat transfer of the considered jet arrays are investigated through an experimental measurement. The results of this measurement are presented in the following.

Fig. 6 shows the temperature distributions on the impingement plate for the s/d of 4.0 and the H/d of 2.0.

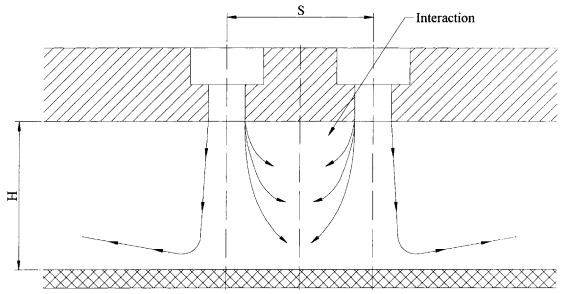

Fig. 4. Jet interference before impingement.

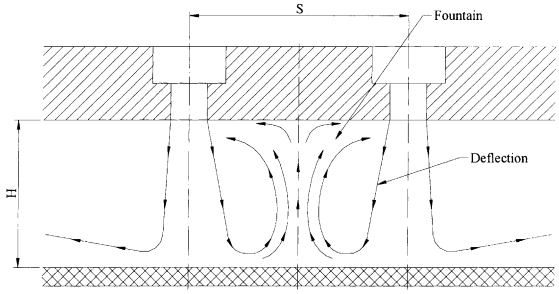

Fig. 5. Jet fountain in a multijet impingement.

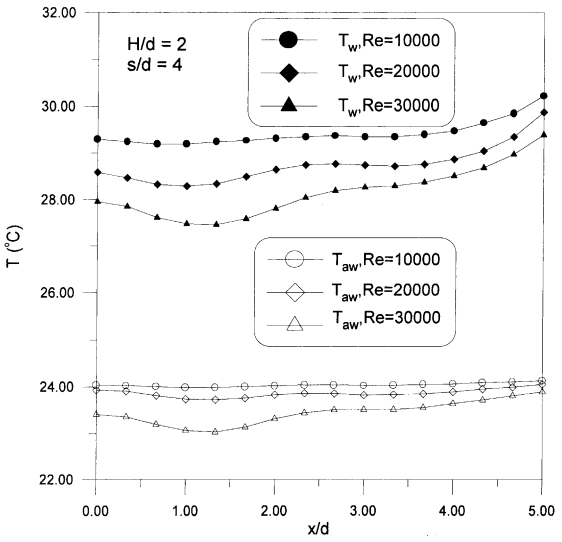

Fig. 6. Temperature distributions.

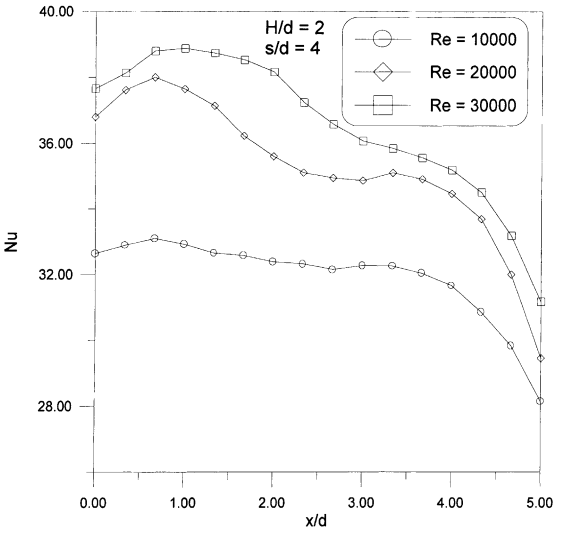

Fig. 7. Local Nusselt number ($H/d = 2$, $s/d = 4$).

For the case with the *Re* greater than 20,000, it shows that a minimum temperature occurs at the x/d of 1.0. The location of the minimum temperature for the multiple jet impingement appears to be very close to that for a single jet impingement [3]. As pointed out in the literature [3], the formation of this minimum temperature is due to the occurrence of the transition point. Before the transition point the jet flow is in the impingement region. As the flow passes through the transition point, the jet flow will be in the wall jet region. For the case with the *Re* of 10,000, the strength of the jet flow is weak, thus the above minimum point does not exist.

Fig. 7 shows the distributions of the local Nusselt number for the same three cases as considered in Fig. 6. In Fig. 7, due to the fountain effect, the heated air is not easy to be expelled from the space near the center jet. Thus the heat transfer near the stagnation point of the center jet ($x = y = 0$) is deteriorated. Besides that, due to the flow acceleration from the impingement region to the wall jet region, there exists a maximum *Nu* at the transition point ($x/d \approx 1$). However, for the case with the *Re* of 10,000, the wall jet is weak and thus this maximum *Nu* is not as clear as that for the case with a high *Re*. As shown in Fig. 7, for the x/d in the range of 2.0–3.5, the decreasing of the *Nu* tends to be sluggish with an increase of the x/d. As indicated in the literature [14,16], due to a high turbulence intensity of the flow at the location of the fountain, the local heat transfer is enhanced. In this work, the temperature distribution is measured along the *x*-axis. As shown in Fig. 1, this measured region is surrounded by the three jets on the right-hand side. Although this flow field is complicated, the fountain effect due to the interaction of the three jets is believed to be the reason causing the flat portion on the curves for the x/d in the range of 2.0–3.5.

Fig. 8 shows a similar result as that in Fig. 7. However, the considered s/d in Fig. 8 is greater than that as considered in Fig. 7. For a larger s/d, the heated air is easier to be expelled from the space near the center jet. Thus, in Fig. 8, the local maximum *Nu* at the x/d of 1.0 disappears. Besides that, the location of the fountain is beyond the measured region, thus the flat portion on the curves cannot be clearly observed. In this analysis, it also found that, for an increase of the H/d and a

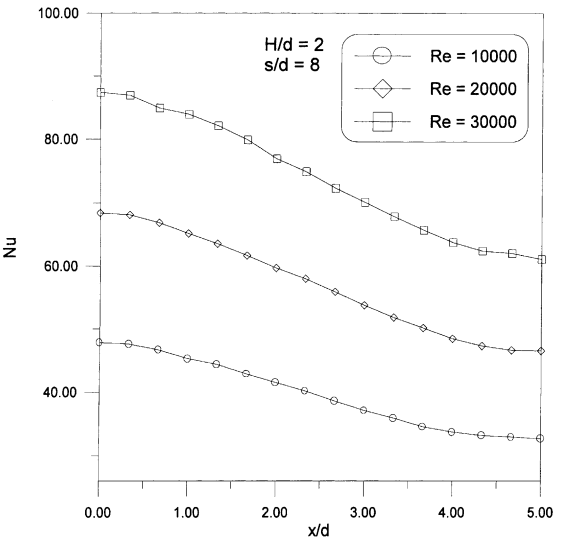

Fig. 8. Local Nusselt number ($H/d = 2$, $s/d = 8$).

decrease of the s/d, the uniformity of the Nu distribution tends to increase. For the sake of brevity, the detailed experimental data illustrating this phenomenon are not shown in this paper.

Figs. 9–12 exhibit the effect of Re on the stagnation Nusselt number ($x = y = 0$), respectively, for the H/d of 2.0, 3.0, 4.0 and 5.0. In Fig. 9, there exists a maximum Nu_{sg} for every curve. To the left of the maximum, the jet fountain is strong. Thus, as the s/d increases, the fountain effect rapidly diminishes. This results in an increase of the Nu_{sg} with the s/d. To the right of the maximum point, due to an increase of the heated area under the jet array, the Nu_{sg} begins to decrease with increasing s/d. Fig. 9 indicates that the optimum s/d, corresponding to the maximum Nu_{sg}, is 8.0 for all the three considered cases. This implies that the Re has very little effect on the optimum s/d. The considered case in Fig. 10 corresponds to the H/d of 3.0. A similar trend as that in Fig. 9 is observed. In Fig. 10, since the corresponding jet height is larger than that as considered in Fig. 9, the strength of the jet fountain becomes weaker. Thus, to the left of the maximum point, as the s/d increases, the fountain effect slowly diminishes and the maximum Nu_{sg} begins to occur at the s/d of 12.0. Metzger et al. [6] performed an experimental measurement to investigate the heat transfer characteristics for in-line and staggered arrays of the circular jets. In their work, 10 rows of jet holes in the chordwise direction (flow direction of spent air) impinging on an isothermal surface were considered. For various values of H/d, Re and s/d, the spanwise averaged Nusselt number was measured. Although the experimental setup in their work is not the same as that in this work, some of their measured data for staggered arrays of impinging jets still

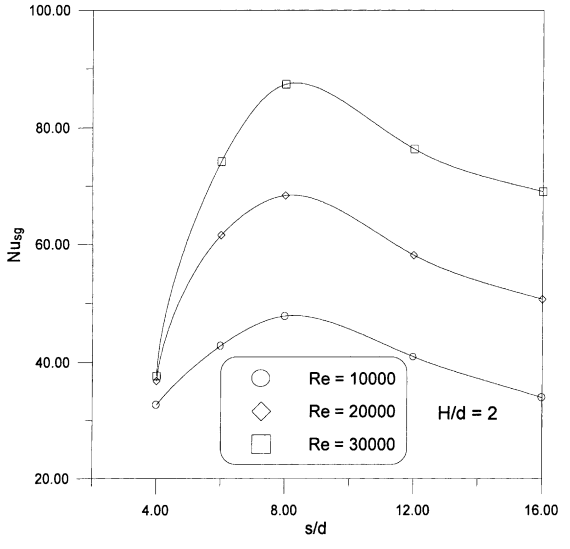

Fig. 9. Effect of Re on Nu_{sg} for H/d of 2.0.

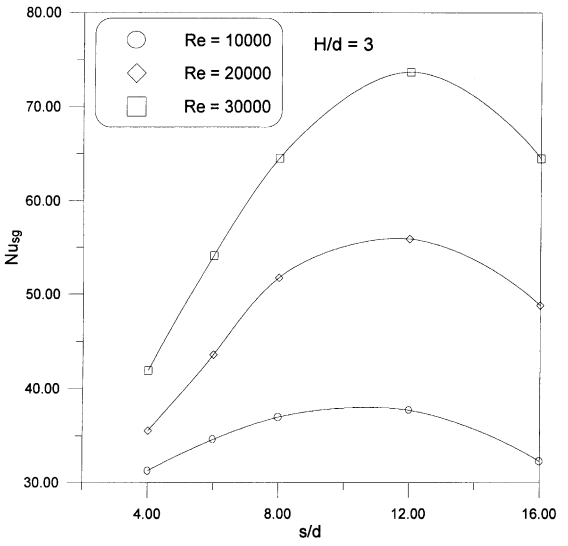

Fig. 10. Effect of Re on Nu_{sg} for H/d of 3.0.

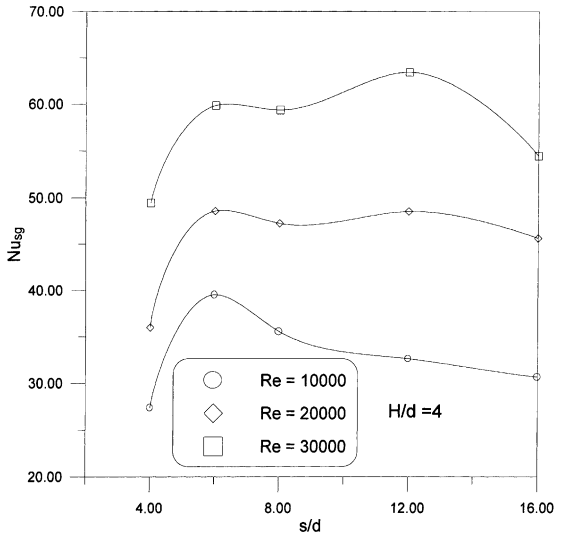

Fig. 11. Effect of Re on Nu_{sg} for H/d of 4.0.

can be used to compare with those as shown in Figs. 9 and 10. Table 1 shows the measured data obtained by Metzger et al. [6] and those obtained in the present work. The comparison indicates that a mean deviation of 10% for the six sets of data between these two measurements.

The Nu_{sg} for the H/d of 4.0 is represented in Fig. 11. As shown in the diagram, for the case with the Re greater than 20,000, there exists two relative maxima of the Nu_{sg} for every curve. The corresponding s/d for the first relative maximum is 6.0 and for the second relative maximum is 12.0. The formation of these two maxima

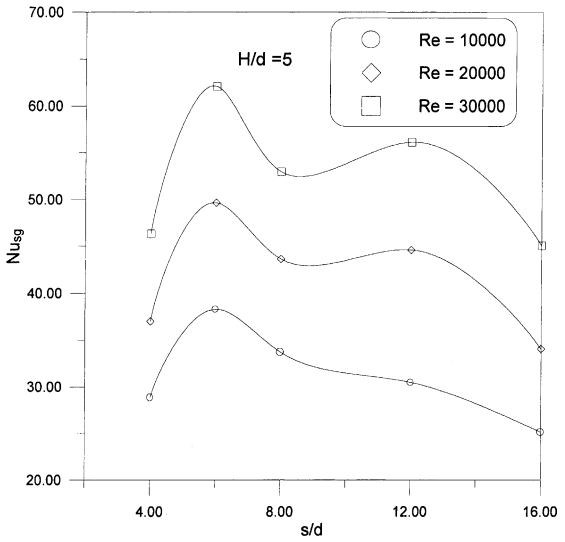

Fig. 12. Effect of Re on Nu_{sg} for H/d of 5.0.

has been roughly interpreted in the beginning of this section. For the case with a small s/d, if both the H/d and Re remain unchanged, an increase of the s/d results in a reduction of the jet interference [17]. Thus the Nu_{sg} increases with the s/d. A further increase of the s/d, a fountain forms. Due to the fountain effect and an increase of the corresponding heated area, the Nu_{sg} will descend. Thus the first relative maximum appears in the diagram. If the s/d is still increased, the strength of the jet fountain will gradually decrease and the Nu_{sg} will rise again. As the s/d exceeds a certain value, the Nu_{sg} will descend and eventually it will approach the value for a single jet impingement. Under this circumstance, the second relative maximum forms. The result shown in Fig. 11 is different from those as shown in Figs. 9 and 10. In Figs. 9 and 10, the first relative maximum of the Nu_{sg}, due to the jet interference before impingement, does not appear in the results. One possibility for this phenomenon could be due to a weak jet interference for the case with a low H/d. Another possibility could be due to the limitation of the experimental apparatus. In this work, the smallest s/d that can be arranged is 4.0. If the first relative maximum of the Nu_{sg} occurs at an s/d less than this value, obviously this point would not be observed in the present results.

As shown in Fig. 11, for the Re of 30,000, the second relative maximum is higher than the first relative maximum. As the Re decreases, the second relative maximum also descends. For the Re of 20,000, the corresponding value of the first relative maximum is almost the same as that of the second relative maximum. In other words, in this case, the heat transfer performance of the jet array with the s/d of 6.0 is almost the same as that with the s/d of 12.0. For the Re of 10,000, the strength of the wall jet is weak, thus the fountain effect is not observable from the present heat transfer data.

Fig. 12 shows the Nu_{sg} for the H/d of 5.0. For a larger H/d, the shear layer would expand wider before jet impingement. As indicated in the result, the jet interference before impingement is very severe, thus the first relative maximum of the Nu_{sg} is quite pronounced. The result also shows that the first relative maximum is higher than the second relative maximum. From a design viewpoint, for the H/d of 5.0, the optimum s/d should be based on the first relative maximum instead of the second relative maximum.

Figs. 13–15 exhibit the Nu_{sg}, respectively, for the Re of 30,000, 20,000 and 10,000. In Fig. 13, it clearly shows that the second relative maximum of the Nu_{sg} decreases with increasing the H/d. As the H/d increases, the corresponding s/d of this second relative maximum also tends to increase and it varies in the range of 8–12. For the jet height (H) larger than $4.0d$, which exceeds the length of the potential core of the jet, the first relative maximum appears at the s/d of 6.0. For the H less than $4.0d$, as explained earlier, the first relative maximum cannot be observed. Fig. 14 exhibits a similar result as that in Fig. 13. However, due to a difference in the Re, the corresponding values of the Nu_{sg} in the former are less than those in the latter. Fig. 15 shows the result for the Re of 10,000. As explained earlier, for the case with a low Re, the strength of the wall jet is weak, thus the fountain effect is not significant. This results in the

Table 1
Comparison of experimental measured data

Non-dimensional parameters	Spanwise averaged Nu at the 2nd row (Metzger et al. [6])	Nu_{sg}
$H/d = 2$		
$Re = 10{,}000$, $s/d = 6.4$	44	42
$Re = 10{,}000$, $s/d = 10.2$	40	45
$Re = 20{,}000$, $s/d = 10.8$	52	60
$H/d = 3$		
$Re = 10{,}000$, $s/d = 6.4$	44	35
$Re = 10{,}000$, $s/d = 10.2$	38	38
$Re = 20{,}000$, $s/d = 10.8$	50	55

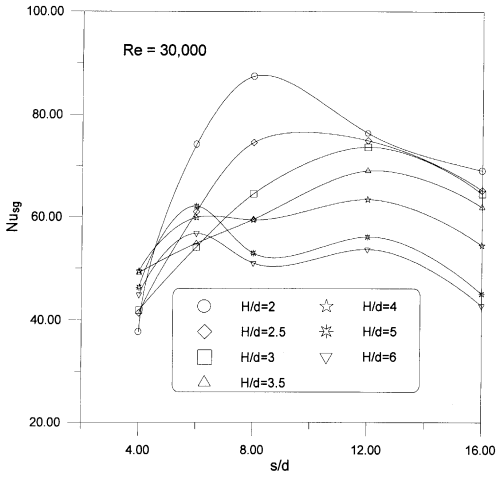

Fig. 13. Nu_{sg} for Re of 30,000.

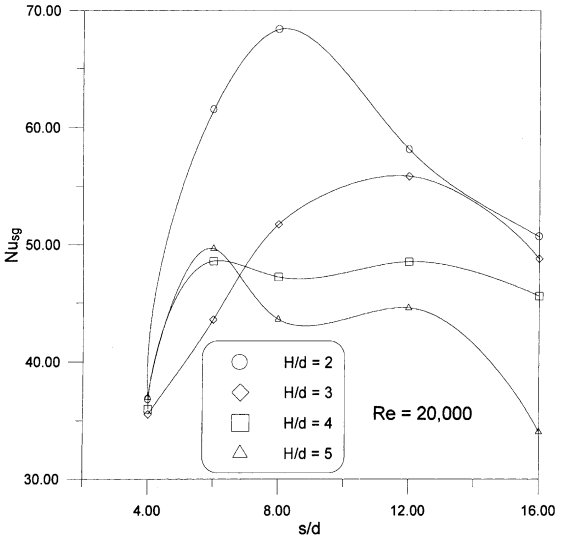

Fig. 14. Nu_{sg} for Re of 20,000.

disappearance of the second relative maximum of the Nu_{sg} for $H/d \geqslant 4.0$.

6. Curvefitting of Nu_{sg}

The experimental data in Figs. 13–15 are correlated by using the following expression:

$$Nu_{sg} = (s/d)e^{\alpha_1+\alpha_2(s/d)}Re^{\alpha}, \tag{3}$$

where

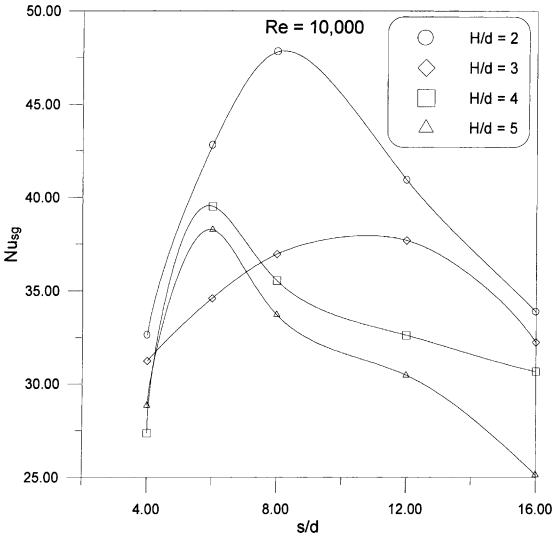

Fig. 15. Nu_{sg} for Re of 10,000.

$$\alpha_1 = \sum_{i=0}^{2}\beta_i(H/d)^i \quad \text{and} \quad \alpha_2 = \sum_{i=0}^{2}\gamma_i(H/d)^i.$$

The coefficients in the above equation and the corresponding errors between the experimental data and correlation results are listed in Table 2.

The same experimental data are also curvefitted by using a high-order polynomial with Re, s/d and H/d as the variables. This polynomial is shown as follows:

$$Nu_{sg} = \sum_{i=0}^{2}\sum_{j=0}^{5} c_{ij}(H/d)^i(s/d)^j, \tag{4}$$

where

$$c_{ij} = \sum_{k=0}^{2} a_{ijk}Re^k,$$

for

$$10{,}000 \leqslant Re \leqslant 30{,}000,$$
$$4 \leqslant s/d \leqslant 16,$$
$$2 \leqslant H/d \leqslant 5.$$

The corresponding coefficients, a_{ijk} , in Eq. (4) are listed in Table 3. The maximum deviation between the measured data and the curvefitting results is 9% and the mean deviation is 3.1%.

7. Conclusions

Jet interference before impingement and jet fountain are two important factors affecting the heat transfer characteristics of the considered jet arrays. The former

Table 2
Coefficients of regression analysis

	$2 \leqslant H/d \leqslant 3.5$ $6 \leqslant s/d \leqslant 16$	$3.5 < H/d \leqslant 6$ $4 \leqslant s/d < 8$	$3.5 < H/d \leqslant 6$ $8 \leqslant s/d \leqslant 16$
β_0	−0.504	−2.627	−4.752
β_1	−1.662	0.546	1.007
β_2	0.233	−0.049	−0.103
γ_0	−0.281	0.132	0.229
γ_1	0.116	−0.093	−0.132
γ_2	−0.017	0.008	0.013
α	0.6	0.4	0.5
max. error	12.9%	13.0%	6.5%
mean error	4.13%	6.43%	3.27%

reduces the strength of the jets, this consequently deteriorates the overall heat transfer. The latter causes a flow recirculation between the fountain and center jet. Due to entrainment effect, the heat transfer of the jet array is also deteriorated.

Two relative maxima of the Nu_{sg} coexist for some of the considered jet arrays with a large Re and a large H/d. The first relative maximum occurs at a smaller s/d and the second relative maximum occurs at a larger s/d. The occurrence of the two maxima can be interpreted by using the current heat transfer data and the previous flow visualization in the literature [13]. For a small s/d, if both the H/d and Re remain unchanged, an increase of the s/d results in a reduction of the jet interference. Thus the Nu_{sg} increases with the s/d. A further increase of the s/d, due to the fountain effect and an increase of the corresponding heated area, the Nu_{sg} will descend. Thus the first relative maximum forms. If the s/d is still increased, the strength of the jet fountain will gradually decrease and the Nu_{sg} will rise again. As the s/d exceeds a certain value, the Nu_{sg} will approach the value for a single jet impingement and the second relative maximum forms.

For a small $Re(\sim 10{,}000)$, if the H/d is large ($\geqslant 3.0$), the strength of the fountain is weak. Thus, the second relative maximum of the Nu_{sg} disappears. For a small H/d (< 3.5), the shear layer expansion in the jet is minor and the jet interference before impingement should occur at a small s/d. In this case, due to the limitation of the experimental apparatus, the first relative maximum of the Nu_{sg} cannot be observed.

From the results of this experiment, for the Re in the range of 10,000–30,000 and the s/d in the range of 4.0–16.0, the optimum s/d for the H/d of 2.0 is 8.0; the optimum s/d for the H/d of 3.0 is 12.0; the optimum s/d for the H/d of 5.0 is 6.0. For the case with the H/d of 4.0, if the Re is 30,000, the optimum s/d is 12.0; if the Re is 20,000, two optimum values of s/d, 6.0 and 12.0 coexist; if the Re is 10,000, the optimum s/d is 6.0.

Table 3
Values of a_{ijk}

a_{ijk}	$i=0$	$i=1$	$i=2$
$j=0$			
$k=0$	2.134E+03	−1.220E+03	1.554E+02
$k=1$	−2.066E−01	1.227E−01	−1.693E−02
$k=2$	3.655E−06	−2.123E−06	2.818E−07
$j=1$			
$k=0$	−1.227E+03	7.166E+02	−9.233E+01
$k=1$	1.192E−01	−7.188E−02	1.002E−02
$k=2$	−2.283E−06	1.343E−06	−1.795E−07
$j=2$			
$k=0$	2.604E+02	−1.533E+02	1.997E+01
$k=1$	−2.458E−02	1.512E−02	−2.136E−03
$k=2$	5.033E−07	−3.001E−07	4.045E−08
$j=3$			
$k=0$	−2.571E+01	1.526E+01	−2.008E+00
$k=1$	2.374E−03	−1.485E−03	2.122E−04
$k=2$	−5.124E−08	3.093E−08	−4.205E−09
$j=4$			
$k=0$	1.203E+00	−7.188E−01	9.541E−02
$k=1$	−1.094E−04	6.935E−05	−1.001E−05
$k=2$	2.462E−09	−1.501E−09	2.056E−10
$j=5$			
$k=0$	−2.156E−02	1.296E−02	−1.732E−03
$k=1$	1.939E−06	−1.243E−06	1.808E−07
$k=2$	−4.511E−11	2.772E−11	−3.820E−12

References

[1] S.V. Garimella, R.A. Rice, Confined and submerged liquid jet impingement heat transfer, ASME J. Heat Transfer 117 (1995) 871–877.
[2] J.A. Fitzgerald, S.V. Garimella, A study of the flow field of a confined and submerged impinging jet, Int. J. Heat Mass Transfer 41 (8–9) (1998) 1025–1034.
[3] J.Y. San, C.H. Huang, M.H. Shu, Impingement cooling of a confined circular air jet, Int. J. Heat Mass Transfer 40 (6) (1997) 1355–1364.
[4] R. Gardon, J.C. Akfirat, Heat transfer characteristics of impinging two-dimensional air jets, ASME J. Heat Transfer 88 (1966) 101–108.
[5] D.M. Kercher, W. Tabakoff, Heat transfer by a square array of round air jets impinging perpendicular to a flat

surface including the effect of spent air, ASME J. Eng. Power 92 (1970) 73–82.
[6] D.E. Metzger, L.W. Florschuetz, D.I. Takeuchi, R.D. Behee, R.A. Berry, Heat transfer characteristics for inlined and staggered arrays of circular jets with crossflow of spent air, ASME J. Heat Transfer 101 (1979) 526–531.
[7] L.W. Florschuetz, R.A. Berry, D.E. Metzger, Periodic streamwise variations of heat transfer coefficient for inlined and staggered arrays of circular jets with crossflow of spent air, ASME J. Heat Transfer 102 (1980) 132–137.
[8] L.W. Florschuetz, C.R. Truman, D.E. Metzger, Streamwise flow and heat transfer distributions for jet array impingement with crossflow, ASME J. Heat Transfer 103 (1981) 337–342.
[9] L.W. Florschuetz, D.E. Metzger, C.C. Su, Heat transfer characteristics for jet array impingement with initial crossflow, ASME J. Heat Transfer 106 (1984) 34–41.
[10] L.W. Florschuetz, Y. Isoda, Flow distributions and discharge coefficient effects for jet array impingement with initial crossflow, ASME J. Eng. Power 105 (1983) 296–303.
[11] L.W. Floschuetz, H.H. Tseng, Effect of nonuniform geometries on flow distributions and heat transfer characteristics for arrays of impinging jets, ASME J. Eng. Gas Turbines and Power 107 (1985) 68–75.
[12] L.W. Floschuetz, C.C. Su, Effect of crossflow temperature on heat transfer within an array of impinging jets, ASME J. Heat Transfer 109 (1987) 74–82.
[13] K.R. Saripalli, Visualization of multijet impingement flow, AIAA J. 21 (4) (1983) 483–484.
[14] A.I. Behbahani, Local heat transfer to staggered arrays of impinging circular air jets, ASME J. Eng. Power 105 (1983) 354–360.
[15] R.J. Goldstein, J.F. Timmers, Visualization of heat transfer from arrays of impinging jets, Int. J. Heat Mass Transfer 25 (12) (1982) 1857–1868.
[16] S.J. Slayzak, R. Viskanta, F.P. Incropera, Effect of interaction between adjacent free surface planar jets on local heat transfer from the impingement surface, Int. J. Heat Mass Transfer 37 (2) (1994) 269–282.
[17] A.M. Huber, R. Viskanta, Effect of jet–jet spacing on convective heat transfer to confined, impinging arrays of axisymmetric air jets, Int. J. Heat Mass Transfer 37 (18) (1994) 2859–2869.
[18] A.M. Huber, R. Viskanta, Comparison of convective heat transfer to perimeter and center jets in a confined, impinging array of axisymmetric air jets, Int. J. Heat Mass Transfer 37 (18) (1994) 3025–3030.